Understanding the apparent stator-rotor connections in the rotary ATPase family using coarse-grained computer modeling

Robin A. Richardson,[1] Konstantinos Papachristos,[2] Daniel J. Read,[3] Oliver G. Harlen,[3] Michael Harrison,[4] Emanuele Paci,[2,5] Stephen P. Muench,[4,5] and Sarah A. Harris[1,5]*

[1] School of Physics and Astronomy, University of Leeds, Leeds, United Kingdom

[2] School of Molecular and Cellular Biology, University of Leeds, United Kingdom

[3] School of Mathematics, University of Leeds, Leeds, United Kingdom

[4] School of Biomedical Sciences, University of Leeds, Leeds, United Kingdom

[5] Astbury Centre for Structural Molecular Biology, University of Leeds, Leeds, United Kingdom

ABSTRACT

Advances in structural biology, such as cryo-electron microscopy (cryo-EM) have allowed for a number of sophisticated protein complexes to be characterized. However, often only a static snapshot of a protein complex is visualized despite the fact that conformational change is frequently inherent to biological function, as is the case for molecular motors. Computer simulations provide valuable insights into the different conformations available to a particular system that are not accessible using conventional structural techniques. For larger proteins and protein complexes, where a fully atomistic description would be computationally prohibitive, coarse-grained simulation techniques such as Elastic Network Modeling (ENM) are often employed, whereby each atom or group of atoms is linked by a set of springs whose properties can be customized according to the system of interest. Here we compare ENM with a recently proposed continuum model known as Fluctuating Finite Element Analysis (FFEA), which represents the biomolecule as a viscoelastic solid subject to thermal fluctuations. These two complementary computational techniques are used to answer a critical question in the rotary ATPase family; implicit within these motors is the need for a rotor axle and proton pump to rotate freely of the motor domain and stator structures. However, current single particle cryo-EM reconstructions have shown an apparent connection between the stators and rotor axle or pump region, hindering rotation. Both modeling approaches show a possible role for this connection and how it would significantly constrain the mobility of the rotary ATPase family.

INTRODUCTION

The rotary ATPase family are highly efficient membrane bound energy conversion machines which can either utilize a proton gradient to produce ATP or, conversely, use ATP to generate a proton gradient.[1] This is achieved through the coupling of two distinct motors; an ATP binding domain, and a membrane bound proton pump. There are three distinct members of the rotary ATPase family. The F_1F_o-ATPases (F-ATPase) are primarily responsible for ATP synthesis, whilst the vacuolar H^+-ATPases (V-ATPase) use ATP hydrolysis to drive proton transport across the membrane [Fig. 1(A)]. In contrast to the mono-directionality in the V-ATPase, the archaeal A-ATPase [Fig. 1(B)] can work in a bi-directional manner by being capable of both proton transport and ATP synthesis depending on the membrane potential. All these systems make use of a rotational mechanism for either proton pumping or ATP synthesis.[2,3]
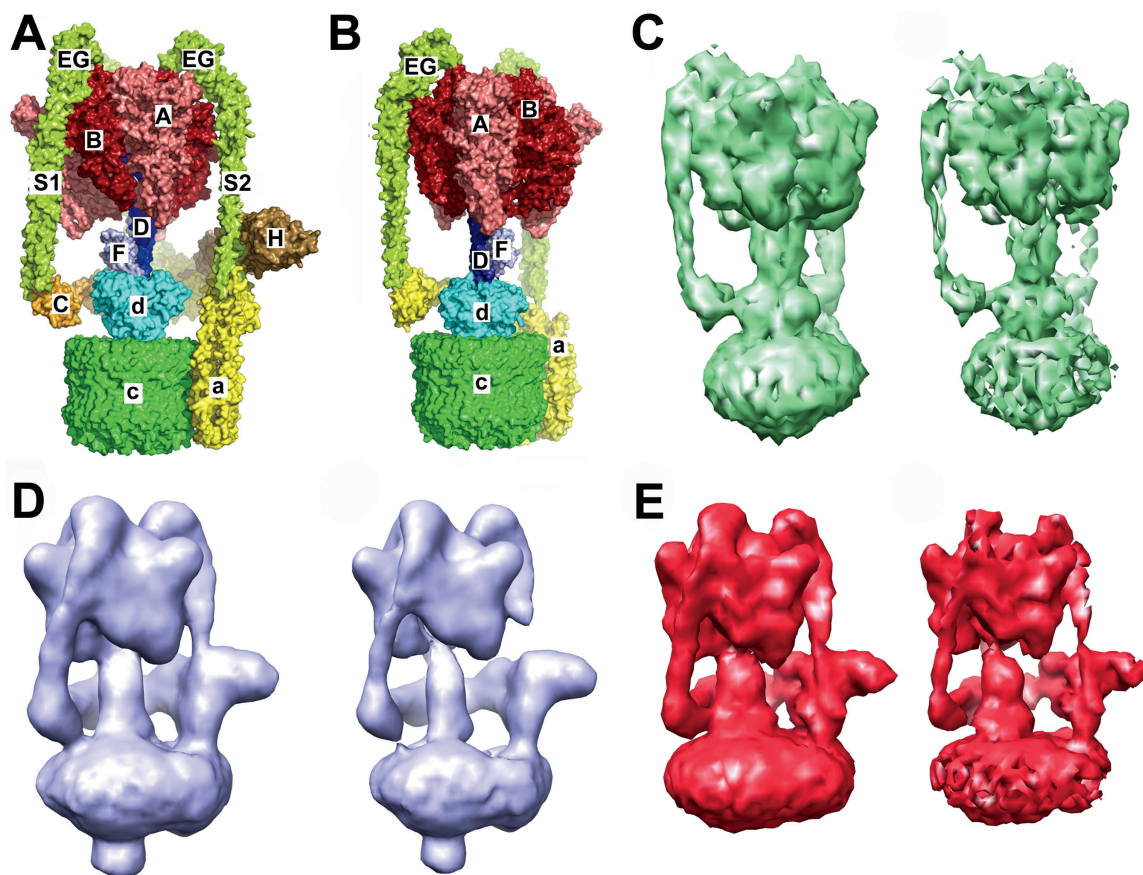
Figure 1

Subunit fitting for the V-ATPase (**A**) and A-ATPase (**B**) complex with those subunits involved in the ATPase motor domain (A/B), stator (E/G/C/H), rotor (D/F/*d*/*a*) and *c*-ring labeled. Single particle cryo-EM reconstruction of the *T. thermophilus* A-ATPase (**C**) *M. sexta* (**D**) and yeast (**E**) V-ATPase and contoured at the recommended level in the EMDB (left) and at a level where the apparent link between stator and rotor axle is removed (right).

For the V-ATPase and A-ATPase (working in proton pumping mode) the soluble A_1/V_1 domain is responsible for ATP turnover. The three catalytic AB dimers function cooperatively and cycle between open (no nucleotide bound), loose (ADP + Pi bound) and tight (ATP hydrolyzing) states.[4] This cycling of the three step motor generates changes in the conformation of the AB dimers, delivering torque to the central rotor, which in turn drives rotation of the *c*-ring.[5,6] Implicit within these motors is the need to fix the ATP hydrolyzing AB domains and the membrane bound *a*-subunit relative to the central rotor axle and proton translocating *c*-ring. This is achieved through a complex stator network that connects the two motors, formed by either two (A-ATPase) or three (V-ATPase) potentially elastic coiled-coil stalk structures (Fig. 1). The F_1F_o ATPase has just one stator connection linking the ATP hydrolyzing F_1 domain and proton translocating F_o domain.

Although significant structure and sequence conservation is seen between many of the comparative subunits in the V- and A-ATPase there are a number of important differences associated with subtle changes in function. An important aspect of the rotary ATP family is the presence of variously sized proton translocating *c*-rings, which are thought to be an adaptation of different prevailing membrane potentials.[7,8] Since the *c*-ring commonly does not contain a multiple of 3, this variation in size results in a symmetry mismatch with the three stroke ATP hydrolyzing/synthesizing domain.[9–11] Since ATP is likely to be limiting within the cellular environment, this symmetry mismatch cannot be overcome by applying constant torque to the central rotor to generate continuous rotation of the *c*-ring. Instead, it has been hypothesized that an elastic linkage between the ATP driven motor and proton translocating pump can act as an energy buffering device.[12–16] This elasticity may exist either in the central rotor axle, the stator network or both. According to this model, the free energy cost of the ATP induced conformational changes are minimized by the inherent elasticity in the system which in turn increases motor efficiency.[17] This flexibility has been reported within crystal structures and electron

microscopy data.[18–20] Moreover, the use of Normal Mode Analysis on the coiled-coil dimeric protein that forms the A-ATPase stator stalk has shown flexing in a radial direction.[21] More recently we have shown using both electron microscopy and an Elastic Network Model (ENM) approach that both the *Saccharomyces cerevisiae* (*S. cerevisiae*) and *Manduca sexta* (*M. sexta*) V-ATPases are capable of flexion of the long axis of the complex such that the V_1 domain is displaced up to $10°$ relative to the V_o domain.[22] Despite the implicit need for the stator connections to fix the $V_1/A_1/F_1$ motor domain and the *a*-subunit relative to the rotating central axle and *c*-ring, there is an apparent second rotor/stator connection evident in all the structures of the complete A- and V-ATPases. This connection will link the EG stator to either the *c*-ring or *d* subunit of the central axle. This linkage removes the ability of the *c*-ring to rotate freely against subunit *a*, during ATP hydrolysis [Fig. 1(C–E)].

Elastic Network models (ENMs) are a widely used class of structure-based coarse-grained models for proteins considering the native structure of the protein as a simple elastic body comprised of a set of nodes connected by springs.[23] In ENMs the coarse-graining step consists of mapping the nodes onto protein structural elements. On the basis of residue-based coarse-graining, there is one bead/node corresponding to each alpha carbon atom. Cut-off distances are usually employed to set interacting nodes. Along with high-resolution X-ray structures, low-resolution structural data from cryo-electron microscopy have been combined with ENMs to investigate biomolecular dynamics.[24,25] Finite Element Analysis (FEA) is used ubiquitously at the macroscopic level for computer aided design within structural engineering applications. Fluctuating Finite Element Analysis (FFEA) is a generalization of FEA to objects which are sufficiently small that thermal fluctuations are non-negligible in magnitude, as described in detail by Oliver *et al.*[26] FFEA represents proteins as viscoelastic materials that deform due to thermal noise. The general equation of motion describing the continuum model is:

$$\rho \frac{D\mathbf{u}}{Dt} = \nabla \cdot \boldsymbol{\sigma} + \mathbf{f} + \nabla \cdot \boldsymbol{\pi}$$

where ρ is the density, $\boldsymbol{\sigma}$ is the continuum stress, $\mathbf{f}$ are additional forces arising from any electrostatic or van der Waals interactions present in the system; and $\boldsymbol{\pi}$ is the stress due to thermal noise. FFEA requires a three-dimensional representation of the shape of the protein as input to the calculations, which may be available either from X-ray crystallography, or low-resolution experimental methods such as small angle X-ray scattering (SAXS) or electron microscopy (EM). In FFEA, the complex shape of the protein is represented by a three-dimensional mesh of elements; the most convenient element shape being the tetrahedron. This mesh can then

be parameterized locally with a bulk modulus, shear modulus, bulk viscosity, shear viscosity, and density. These parameters conceptually describe the cumulative effect at the continuum level of all the local atomic interactions. Once these parameters have been defined, the trajectory describing the changing shape of the protein due to thermal fluctuations can be calculated by iteratively integrating Newton's equations of motion over short time steps and moving each node of the mesh accordingly. The calculation is analogous to conventional molecular dynamics (MD), but the forces on each node within the mesh are derived from continuum mechanics equations rather than a pairwise particle based forcefield.

FFEA can use low-resolution experimental data as input to the calculations, which is particularly useful for proteins whose atomistic structure is still unknown. Since it operates in the continuum limit, it has no upper length scale, and is sufficiently coarse-grained to enable simulations of very large protein structures to be performed for long (e.g. µs) timescales. FFEA contains a dissipative viscous term in addition to elastic stresses, which enables the stochastic nature of the solvent environment to be represented. FFEA can be readily generalized to include any intermolecular forces relevant to biomolecular dynamics, such as van der Waals and electrostatics interactions, so long as the necessary force-field parameters can be obtained. In the current work, the FFEA model used contains a homogeneous elastic term to model the energy penalty associated with deviations from the EM derived structure, and a viscosity describing dissipation in the interior of the protein.

FFEA produces a dynamical trajectory which represents the motion of the protein. The model is parameterized by continuum parameters such as modulus and viscosity. In contrast, in their most common implementation elastic network models are parameterized by spring constants and cut-off distances which affect the connectivity of nodes. They are usually "solved" using normal mode analysis, which does not yield an explicit dynamical trajectory, but rather the eigenmodes of the protein displacement. In principle, it would be possible to add dissipation to the harmonic spring interactions within an ENM scheme to mimic viscosity, and then use Langevin dynamics to simulate a protein trajectory. Likewise, a typical set of displacements (without dynamics) of an FFEA model could be obtained by Monte Carlo sampling, and normal mode analysis may also be possible (though FFEA is, by construction, weakly non-linear). In the present work we use and compare the published implementation of FFEA[26] and normal mode analysis of an ENM model. We use both ENM and FFEA to provide insight into the flexibility and dynamics of the rotary ATPase family in the presence and absence of the apparent linkage. For this particular system, to which both ENM and FFEA are applicable, we have the opportunity to investigate whether the new continuum simulation method (FFEA) correlates well with
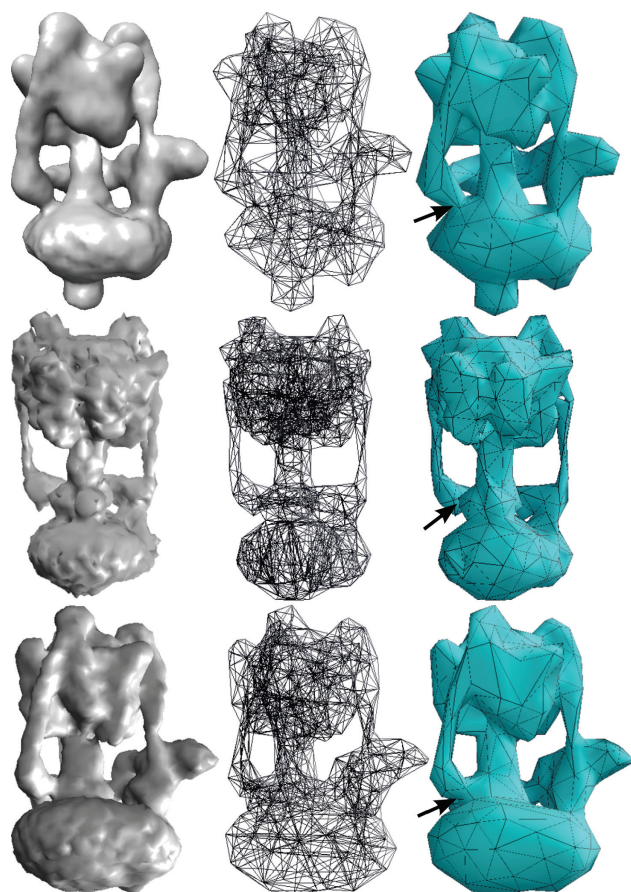
Figure 2

The single particle cryo-EM map (left) versus FFEA models (centre and right) for the *M. sexta* V-ATPase (row **A**), the *T. thermophilus* A-ATPase (row **B**), and the *S. cerevisiae* V-ATPase (row **C**). The location of the apparent connection between the stator network and rotor axle is indicated on each FFEA representation via an arrow.

the more common ENM approach. We subsequently show how the linkage observed in cryo-EM density maps has a significant impact on the inherent modes of flexibility available to the system.

METHODS

The *M. sexta* V-ATPase (EMD-1590 at 17 Å resolution), *S. cerevisiae* V-ATPase (EMD-5476 at 11 Å resolution), and the *T. thermophilus* A-ATPase (EMD-5335 at 9.7 Å resolution) maps were downloaded from the EMDB database. Using the isolevels recommended by the authors in each case, finite element meshes were constructed using NETGEN,[27] as shown in Figure 2.

We performed Fluctuating Finite Element (FFEA) analysis simulations for each of these structures for 4 μs, using the simulation parameters listed in Table I.

The choice of Young's modulus was taken from the lower end of the experimentally determined range for

Table I
Simulation Parameters for FFEA Calculations

Density	1500 kg m^{-3}
Young's modulus	338.8 MPa
Poisson's ratio	0.41
Shear viscosity	1 mPa s
Bulk viscosity	1 mPa s
Time step	5 fs
Temperature	290 K

lysozyme[28] in order to accentuate flexibility. The viscous parameters were taken to be the same as for water. The density parameter was chosen to be the average density of biomolecules.[29,30] The choice of viscous parameters and density affect the time scale of the simulation, and the manner in which the model explores conformational space, but they do not affect the range of configurations available to the protein in the model (i.e. the modes). Modifying the Young's modulus will alter the amplitude of the modes, but not the resultant eigenvectors themselves (except where the deformation is large and non-linear). Test simulations with a 20% difference in Young's modulus were run showing the eigenvectors to be largely unchanged; the Poisson ratio also has only a weak effect on the modes. As with ENM, it is the shape and topology of the protein that determines the modes of motion in FFEA.

The apparent connections between the stator and rotor were then severed, and the simulations repeated. This stator/rotor disconnection was produced by removing a small amount of matter from the connecting area, thus producing a new topology for each motor in which this connection is completely severed.
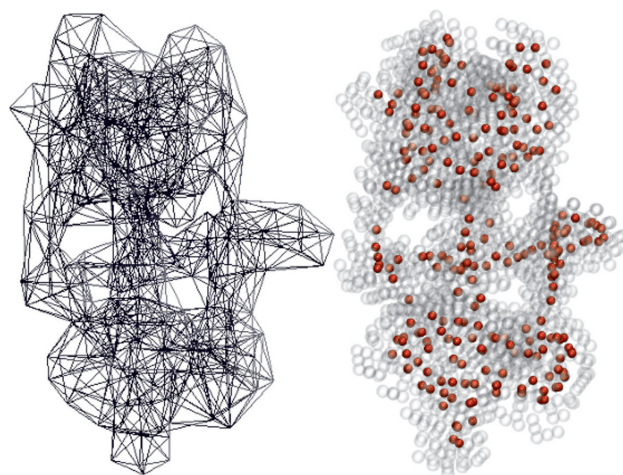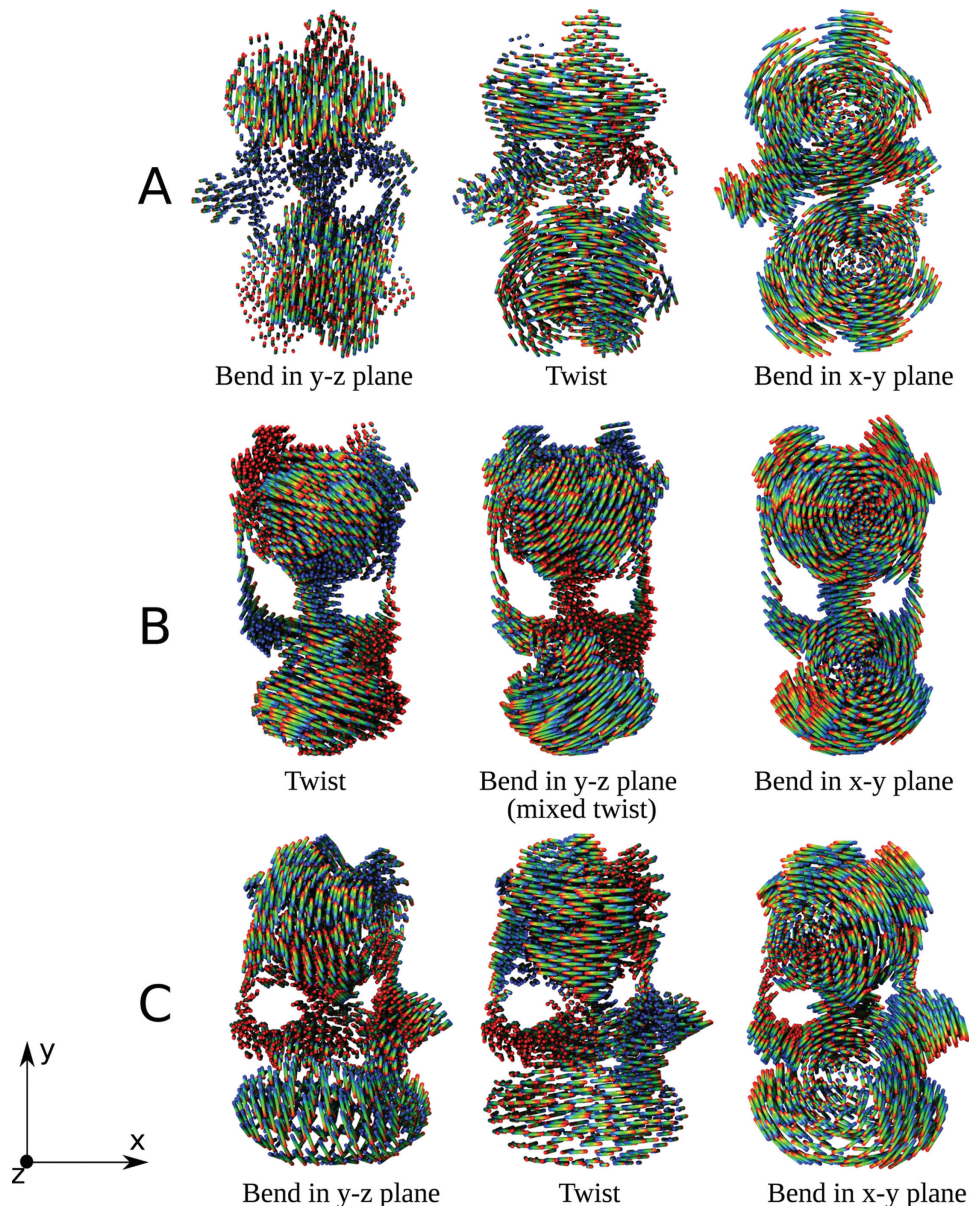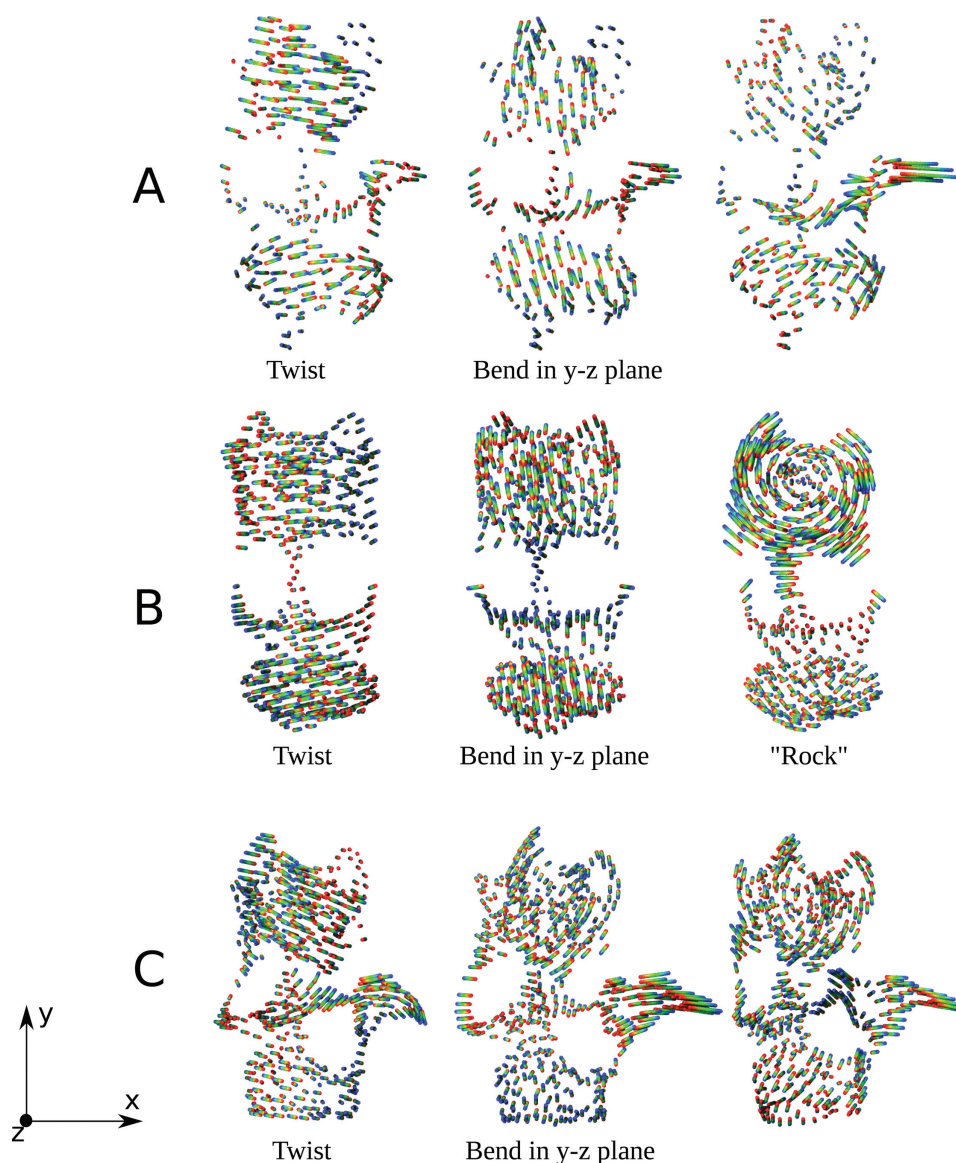

Figure 3

Continuum model showing the FE mesh (left) and embedding the ENM pseudo-particle structure (red) inside the FFEA continuum mesh (grey) represented here by the nodes of the finite elements (right).

Figure 4

First three modes of the FFEA model for the *M. sexta* V-ATPase (row **A**), the *T. thermophilus* A-ATPase (row **B**), and the *Saccharomyces* V-ATPase (row **C**). Colors represent time range of motion, with red indicating the start of the motion and blue indicating the end.

For the ENM normal-mode analysis calculations, the *M. sexta* V-ATPase and *T. thermophilus* A-ATPase have been coarse-grained into a total of 250 beads using a topology-preserving algorithm[31] to capture the overall shape and topology of the complexes. For the *S. cerevisiae* V-ATPase coarse-graining carried out for individual subunits resulted in a 256-bead representation. The beads were connected by springs with spring constant as described by Stember and Wriggers.[32] The Hessian matrix and corresponding eigenvectors were calculated using the Python-based script MODEHUNTER.[32]

The quasi-harmonic normal modes were extracted from the FFEA trajectories using Principal Component Analysis.[33] The first six trivial modes, which describe the overall translation and rotation of the system, were removed prior to the PCA. To compare FFEA with ENM, the ENM structure was aligned within the finite element mesh by minimizing the square of the total pair-pair separation distance between all ENM pseudo-particles and FFEA nodes. This minimization was achieved by sampling many random translations and rotations of the ENM structure. The probability of accepting a new configuration was given by the Boltzmann probability

Twist   Bend in y-z plane

Twist   Bend in y-z plane   "Rock"

Twist   Bend in y-z plane

Figure 5

First three modes of the ENM model for the *M. sexta* V-ATPase (row **A**), the *T. thermophilus* A-ATPase (row **B**), and the *S. cerevisiae* V-ATPase (row **C**). Colors represent time range of motion, with red indicating the start of the motion and blue indicating the end.

$P = \exp(-dE/kT)$ where dE represents the change in the "energy penalty" of the configuration (the total pair-pair distance squared) resulting from that step, and T is a scaling energy analogous to thermal energy in a real system. The purpose of this artificial "temperature" is to allow the structure to sample the whole configurational space and find the global minimum. The temperature was slowly reduced, allowing the system to settle with the optimum alignment of the ENM structure within the FFEA structure.

Once the alignment was converged, each pseudo particle of the ENM structure was assigned to its local (containing) element in the continuum mesh, as shown in Figure 3. The barycentric coordinates of the particle within that local tetrahedron were calculated, and could then be used to map the new position of the particle in all subsequent frames. In this way the motions of the FFEA derived modes were mapped onto the ENM structure, allowing a direct comparison to be made between the two models.

FFEA was also used to investigate the effect of severing the rotor-axle (D from *d*, in Fig. 1) on the modes of the *S. Cerevisiae*. The disconnection was done as previously, but the interface at the cut was now simulated as two interacting van der Waals (vdW) surfaces. The vdW interaction was modeled as the integral of the Lennard-
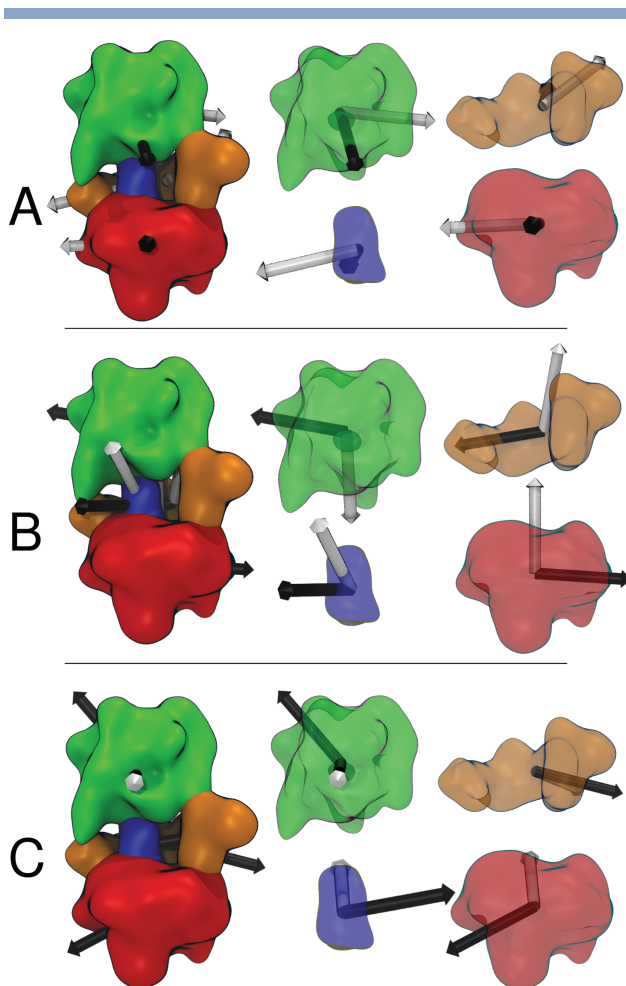
Figure 6

The mobility of four sections of the FFEA representation of *M. sexta* V-ATPase, divided by motor domain (green), rotor (blue), *c*-ring (red) and the remainder of the C, H and *a* subunits (orange), for the first three modes (**A**, **B**, and **C**, respectively). The white arrow shows the normalized rotational velocity vector of that section, and the black arrow shows the motion of the centre of mass during the motion.

Jones (LJ) force over all interacting faces in the mesh. Three simulations of the rotor-axle disconnection were then run, with the vdW surface interaction energy set to 10^{12} Jm^{-4}, 10^{13} Jm^{-4}, and 10^{14} Jm^{-4}. For comparison, consider that an interaction energy of 10^{13} Jm^{-4} with an interacting surface area of 10 nm^2 corresponds to a total interaction energy of order k_BT energy. The LJ equilibrium separation distance was chosen to be 5 Å, as this was the size of the gap after severing.

Similarly, the *S. Cerevisiae* was severed along the interface of its V$_o$ (*c*, *a* and *d*) and V$_1$ (motor domain, D, H, and stators) domains, and the C subunit. These three parts were then allowed to interact via a vdW surface interaction, until dissociation. As the V$_o$ domain is embedded in the membrane, its lower half has been pinned in place by immobilizing the corresponding nodes. The exterior sol-

vent viscosity was chosen to be 10^{-6} Pa s (this is 1000 times smaller than that of water to increase the rate of exploration of conformational space). The LJ equilibrium separation distance was again taken to be 5 Å, and the surface interaction energy to be 10^{15} Jm^{-4}. The separation distance between the centres of mass of the V$_o$ and V$_1$ domains with time was then calculated.

RESULTS

Comparison of FFEA and ENM dynamics

We performed 4 µs FFEA simulations for the *M. sexta* and *S. cerevisiae* V-ATPases and the *T. thermophilus*
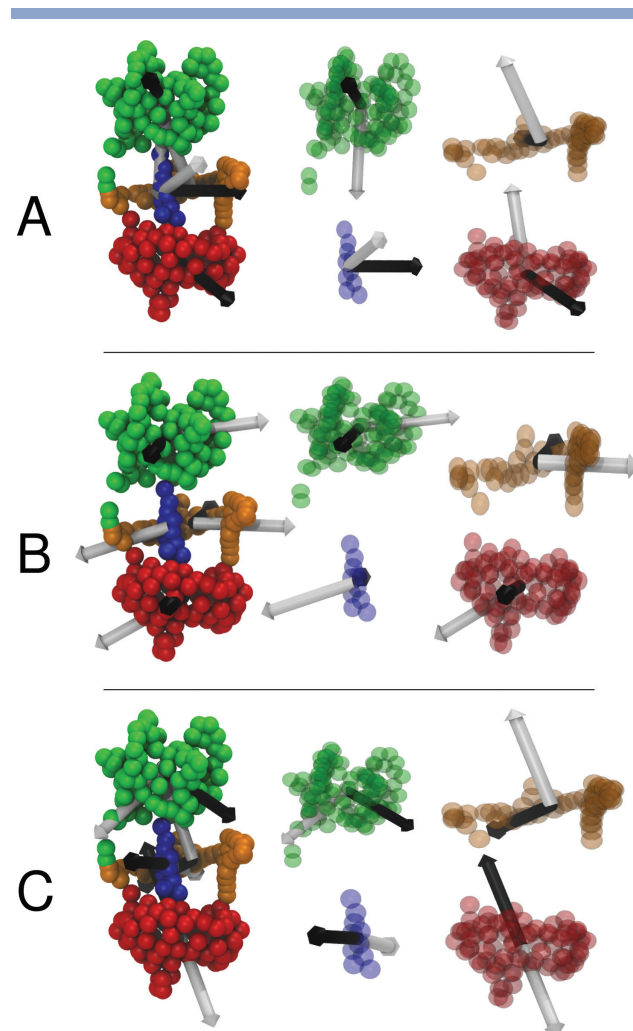

Figure 7

The mobility of four sections of the ENM representation of *M. sexta* V-ATPase, divided by motor domain (green), rotor (blue), *c*-ring (red) and the remainder of the C, H and *a* subunits (orange), for the first three modes (**A**, **B**, and **C**, respectively). The white arrow shows the normalized rotational velocity vector of that section, and the black arrow shows the motion of the centre of mass during the motion.
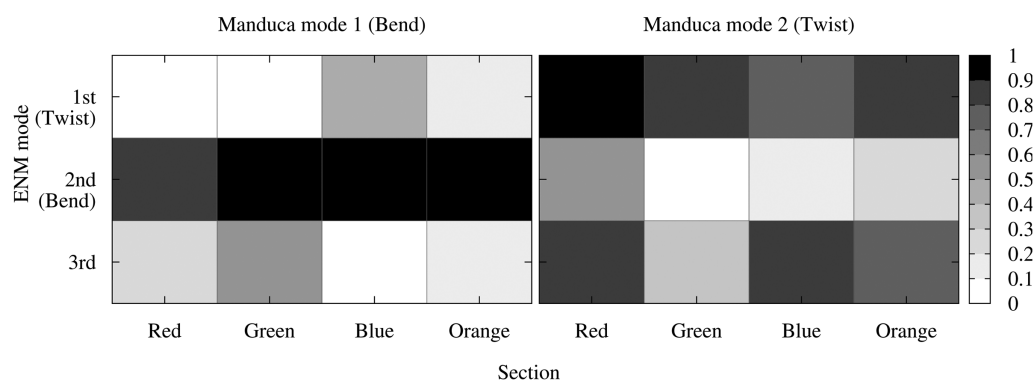
Figure 8

A comparison of the agreement in mobility profile of the four motor sections (as shown in Figs. 6 and 7) for the first two FFEA modes and first three ENM modes of *M. sexta* V-ATPase. [Color figure can be viewed in the online issue, which is available at wileyonlinelibrary.com.]

A-ATPase, with and without the apparent connection between the stator and rotor axle, and extracted the major modes of flexibility from the trajectories using PCA. For the trajectories obtained with both stator connections intact, we compared the motions obtained from FFEA with those calculated with a conventional ENM. The PCA showed that the first two most significant non-trivial modes for the connected mesh corresponded to twisting and bending in both the FFEA and ENM (see Figs. 4 and 5 and Supporting Information Movies S1–S4).
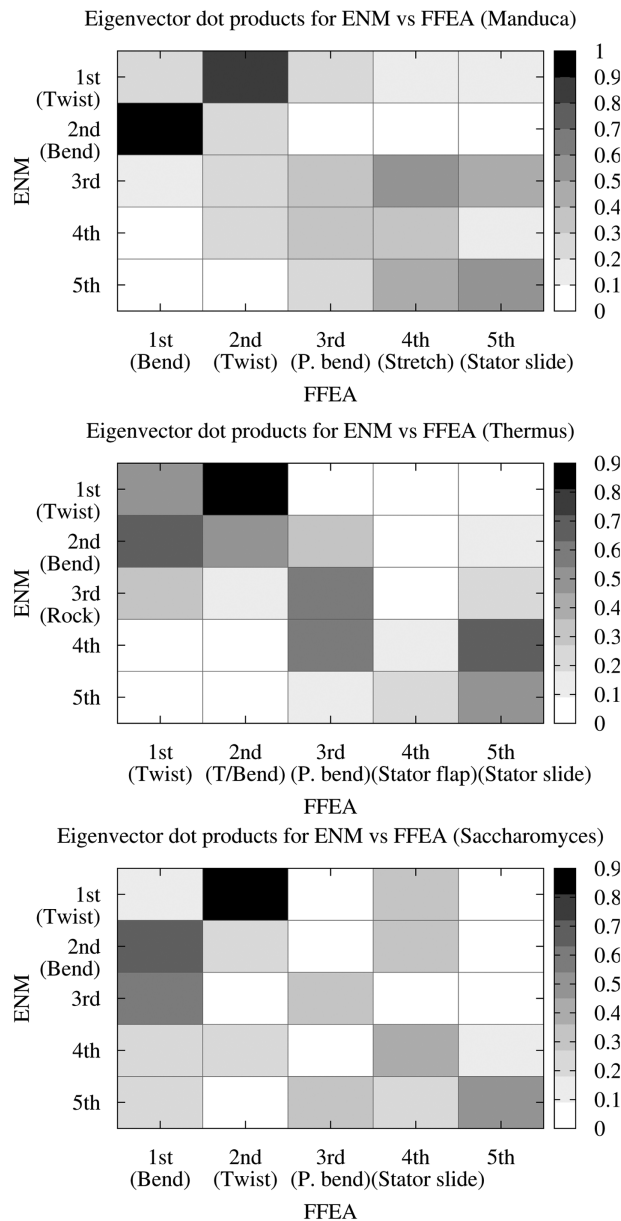
A quantitative comparison of the ENM and FFEA model was obtained by calculating the dot products of each eigenvector obtained from the ENM with each eigenvector extracted from the FFEA trajectories using PCA, as shown in Figure 9. The differences in shape of the ATPase models in Figures 4 and 5 are due to the fact that the FFEA mesh contained more nodes than the number of pseudo-particles in the ENM, and this is accounted for by our alignment procedure (see Methods). Nevertheless, Figure 9 shows that there is a clustering of high correlation between modes close to the diagonal, indicating that similar modes of flexibility of the ATPases are predicted by both the ENM and FFEA calculations. Although the agreement between the two modeling methods is reduced for the higher order modes in each of the three ATPases, these modes have far smaller amplitudes (Fig. 10) and so we conclude that the major modes of flexibility captured by the two complementary methods are comparable. Subtle differences in the ordering of these modes are due to the contrasting treatment of local elasticity by ENM and FFEA. The characteristic "springs" of the ENM are one-dimensional objects and, in isolation, exhibit little torsional resistance, whereas the volume elements of FFEA strongly resist torsion as well as extension. This is particularly evident in the central stalk region of the simulations, which contain only a few elements or springs; in this region the FFEA simulations are more resistant to torsion than the corresponding ENM simulation. As a result, in the *M. sexta* V-ATPase, the bending mode dominates in the FFEA, whereas the twisting motion dominates in the ENM.

Further insight into the agreement between FFEA and ENM models of the ATPase protein complex can be obtained by considering the relative motions of the different subunits of the motor. Figures 6 and 7 show the bulk mobility of four separate domains of the *M. sexta* V-ATPase motor, in terms of the rotational velocity vector, and the centre of mass velocity vector, for the first three modes in the FFEA and ENM representations. Figure 8 shows a quantitative comparison of the agreement in mobility between the four sections in the two representations, and demonstrates that, in agreement with the dot products presented in Figure 9, the major modes of flexibility of the ATPase are conserved between the ENM and FFEA.

Comparison of the FFEA dynamics in the *M. sexta* and the *S. cerevisiae* V-ATPases and the *T. thermophilus* A-ATPase

The eigenvalue spectrum obtained for the six FFEA models is shown in Figure 10. Since larger eigenvalues are obtained for the *T. thermophilus* A-ATPase, we conclude that this is the most flexible of the three motors. The *S. cerevisiae* V-ATPase is marginally more flexible than that from *M. sexta* during FFEA. The differences between the two V-ATPase reconstructions may be attributed to species variation and/or differences in resolution (11 Å rather than 17 Å) with a decreased volume associated with more detailed structural information permitting larger amplitude thermal fluctuations to occur within the FFEA model. Significant topological changes can affect the output of the simulations therefore it is important to verify the effect of changes in resolution.

Eigenvector dot products for ENM vs FFEA (Manduca)

Eigenvector dot products for ENM vs FFEA (Thermus)

Eigenvector dot products for ENM vs FFEA (Saccharomyces)

Figure 9

Comparison of the ENM modes with the FFEA modes for the *M. sexta* V-ATPase, *T. thermophilus* A-ATPase and *S. cerevisiae* V-ATPase. [Color figure can be viewed in the online issue, which is available at wileyonlinelibrary.com.]

Figure 13 shows the mode comparison between the high resolution EMD-5335 structure (9.7 Å resolution) and the low resolution EMD-1888 structure[34] (16 Å resolution). This is a rather substantial change in resolution, but as expected the low order modes appear broadly unchanged. It is clear that the first three modes of the *T. thermophilus* A-ATPase are resilient to changes in resolution. Both simulations appear to agree on a fourth mode, although not on the ordering (fourth for the EMD-1888, fifth for the EMD-5335).

PCA mode eigenvalues for all simulations
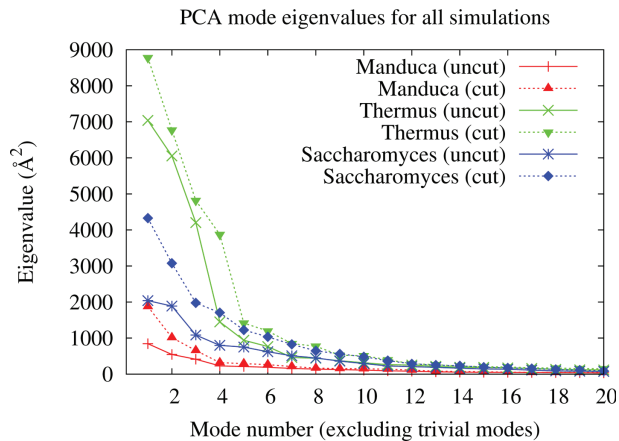
Figure 10

Eigenvalues for the first 20 PCA modes in the three "cut" and three "uncut" simulations.

The cumulative proportion of the eigenvalues of the first five modes relative to the total for all modes is given in Figure 12. This shows that the lower modes in the flexible topologies (those with a severed stator-rotor connection) represent a significantly larger proportion of their total dynamics than the more rigid, uncut topologies.

Dot-product matrices comparing the eigenvectors of the *M. sexta* and *S. cerevisiae* V-ATPases [Fig. 13] show that the major modes of flexibility of the two structures are almost identical. Comparing the eigenvectors of the *M. sexta* and *S. cerevisiae* V-ATPases with the *T. thermophilus* A-ATPase [Fig. 13, respectively] shows that the twisting mode is promoted in the A-ATPase relative to the two V-ATPases, presumably because the former

Eigenvector dot products for Thermus High Res vs Low Res
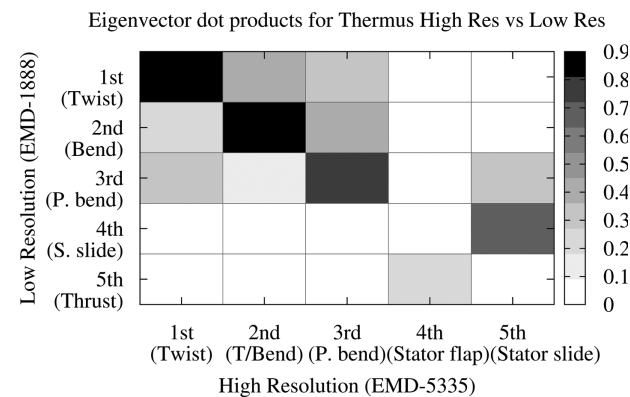
Figure 11

Comparison of the FFEA modes for the *T. thermophilus* A-ATPase at 16 Å resolution (EMD-1888) and 9.7 Å resolution (EMD-5335). [Color figure can be viewed in the online issue, which is available at wileyonlinelibrary.com.]
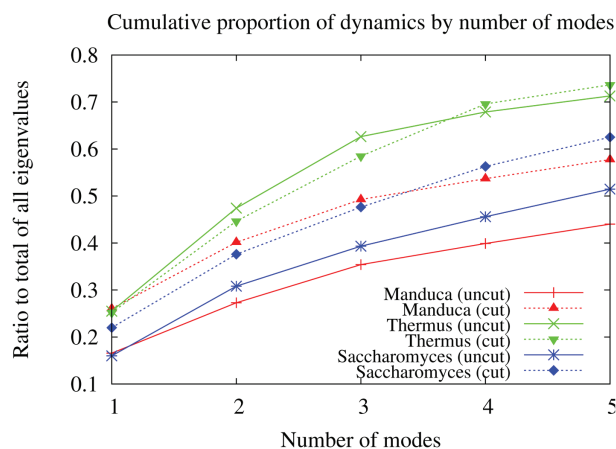
Figure 12

Proportion of the total dynamics represented by the first five modes of each simulation trajectory.

contains only two stator filaments as opposed to three in the V-type complex. This result indicates the importance of connectivity within the structure of the rotary ATPases to the dynamics of these molecular motors.

Changes in rotary ATPase FFEA dynamics with stator-rotor connectivity

We then used FFEA simulations to explore the effect of disconnecting stator filament 1 [Supporting Information S1 in Fig. 1(A)] from the rotor (as indicated in Fig. 2) on the dynamics of the three rotary motors. A quantitative comparison of FFEA simulations with and without the connection was obtained by performing PCA on the FFEA trajectories. Comparing the eigenvalue spectrums obtained (see Fig. 10) shows that all three motors have enhanced flexibility when this connection is severed. Taking dot products between the eigenvectors extracted by PCA, Figure 13 shows that for *M. sexta* the original twist [Fig. 4(A), mode 2] and *x-y* bend [Fig. 4(A), mode 3] motions become mixed when the connection is severed, but that the most important dynamic mode (bending in the *y-z* plane) persists. For the *T. thermophilus* A-ATPase, all of the top three modes of flexibility are preserved when the connection is severed, as shown in Figure 13 (see Supporting Information movies S5 and S6). Since this motor has only two stator connections as opposed to three, its stiffness is dominated by the central rotor axle. Consequently, changes to stator connectivity have a negligible effect on the dynamics. However, for the *S. cerevisiae* V-ATPase, the major modes of flexibility are more severely affected by severing the stator-rotor connection. In all three of the principal modes, the flexibility is dominated by motion of the unconnected stator local to the point of severance. In the first mode, this motion appears to be coupled to a rotation of the *c*-ring, the second

mode is similar to the y-z plane bending mode dominant in the connected system and the third involves a twist of the motor around the central rotor axle. However, since the large flexibility of the stator local to the severance point dominates in all of these modes, the magnitude of the correlations quantified by the dot-product matrices is reduced [see Fig. 13]. In the higher resolution *S. cerevisiae* V-ATPase in which the stator elements of the structure are better defined, stator 1 becomes sufficiently flexible when it is disconnected from the central axle that its independent motion dominates the dynamics of the motor, and the collectiveness of the dynamics across all three of the top modes is reduced. Nevertheless, the principal modes of the disconnected *S. cerevisiae* V-ATPase do still retain aspects of the bending and twisting modes present in all other systems investigated.

FFEA also allows the investigation of the effect of the rotor-axle connection on the modes of the system. Figure 14 shows the effect on the "P. bend" mode of the rotor dissociating from the axle for different dissociation energies. Interestingly, the first two modes (bend and twist) are unaffected by the energy of interaction between the D and d subunits (as labeled on Fig. 1).

In order to further test the FFEA model for its wider application, we investigated how well it could model the V-ATPase dissociation mechanism. Finally, Figure 15 shows the results of the FFEA simulation of V_o, V_1 and the C subunit dissociating. The separation distance between the centres of mass of V_o and V_1 fluctuates as the two domains detach and reattach. The C subunit breaks away first, weakening the cohesion of the structure which finally dissociates completely.

DISCUSSION

A common method for visualizing low frequency motions of large proteins is Elastic Network Modeling, in which each pseudo-atom is linked to its neighboring particle by a "spring" with a defined elasticity. A new but complementary method for looking at intrinsic flexibility in biomolecules is Fluctuating Finite Element Analysis (FFEA), in which the macromolecule is described by a thermally driven viscoelastic continuum with a local elasticity dependant on known biochemical parameters. In order to test how well these two approaches can be used to elucidate intrinsic flexibility within the rotary ATPase family of protein complexes we have calculated the dynamics of two species variable V-ATPases and one A-ATPase using both ENM and a continuum model, and compared the resulting eigenvectors quantitatively by taking dot products. The two modeling methods agree strongly, and show that bending and twisting of the motor dominates the dynamics in both cases (Figs. 4–6).

The single particle cryo-EM reconstructions for the V and A-ATPase have revealed an intricate network of
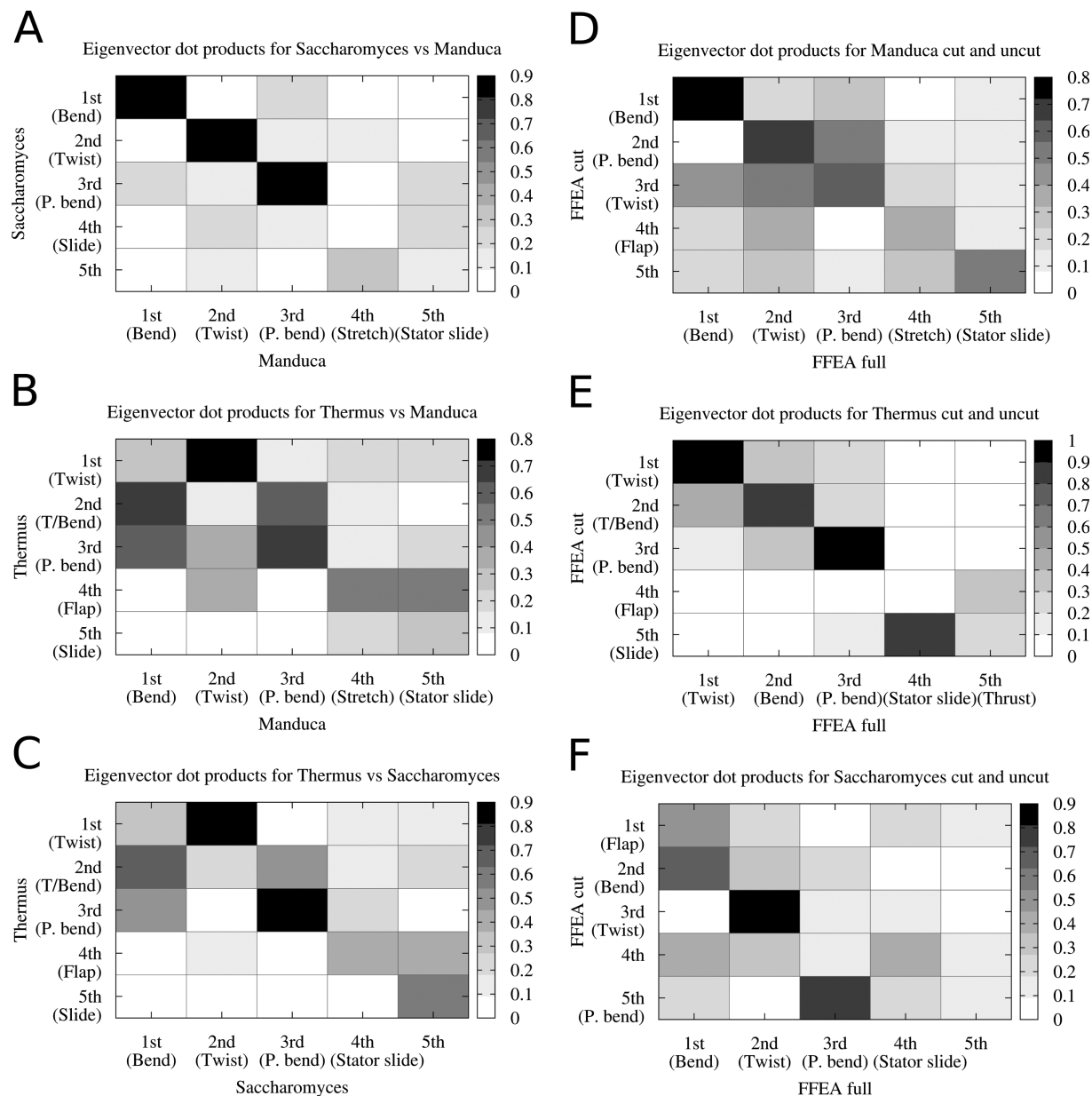
Figure 13

Left: comparison of the FFEA modes for the *M. sexta* V-ATPase with those of *S. cerevisiae* V-ATPase (**A**), *M. sexta* V-ATPase with *T. thermophilus* A-ATPase (**B**), and *S. cervisiae* with *T. Thermophilus* (**C**). Right: comparison of the FFEA modes for the *M. sexta* V-ATPase (**D**), the *T. thermophilus* A-ATPase (**E**), and the *S. cerevisiae* V-ATPase (**F**) with and without the stator connection. [Color figure can be viewed in the online issue, which is available at wileyonlinelibrary.com.]

subunits that contribute to the stator of each motor, which allow for the efficient power transfer between the two motor domains.[35–37] However, implicit within these motors is the need for the central rotor axle and *c*-ring to be able to rotate relative to the V_1/A_1 motor domain and stator network. Importantly, in addition to the *a/c* interface that is proposed to be the site of proton transport, there is a clearly visible connection between stator 1 in both the A-and V-ATPase and either the central rotor axle or the *c*-ring (Fig. 1). The inter-

face between the *a/c* subunits is still poorly defined due to the lack of structural data on subunit *a*, however, the role of this interface within the family of rotary ATPases in proton transport makes it likely to be a transient interface whereby the *c*-ring can rotate against the *a* subunit. The second interface which is seen in the reconstructions involves a connection between stator 1 and the *c*-ring or rotor axle and its role is unknown. This connection can be seen in both the cryo-EM and negative stain reconstructions and is found in a region
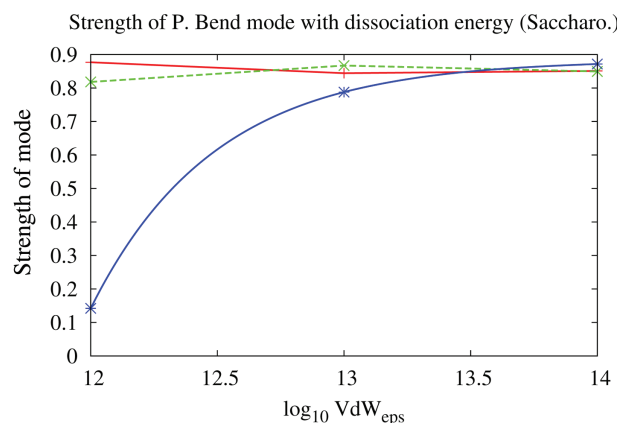
Figure 14

Strength of *S. cerevisiae* V-ATPase perpendicular bend mode with increasing dissociation energy between rotor and axle. The first, second and third modes are represented by the red, green and blue lines respectively.

away from the detergent which covers the membrane bound regions. In order to see how this connection may influence the inherent flexibility within the complex and the ability of these large complex macromolecular motors to function we used a continuum modeling approach to calculate how the major modes of flexibility are affected by severance of this connection. While disconnecting stator 1 from the central axle increases the flexibility of all three motors, for the higher resolution *S. cerevisiae* structure the major modes of flexibility become dominated by the local motion of the stator, and the collective nature of the dynamics is lost.

The reasons for the linkage between the stator network and the central rotor axle or rotor ring are yet to be
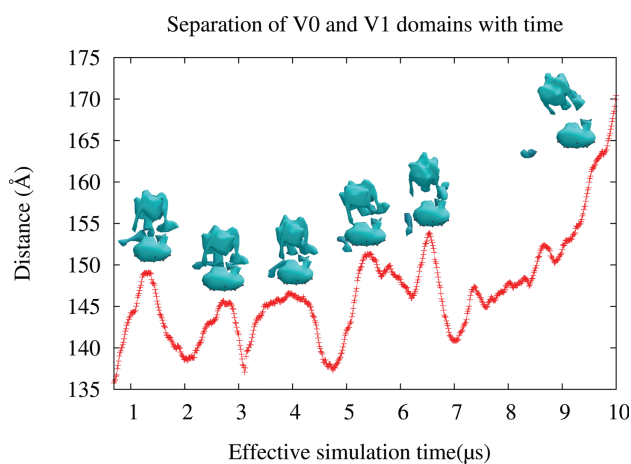

Figure 15

The separation of the V_o and V_1 domains of the *S. cerevisiae* with simulation time during dissociation. Simulation snapshots to illustrate the configuration of the V_o, V_1 and C subunit during the simulation.

determined but there are a number of possible roles that this may play. The first possible role is to maintain the *a* subunit *c*-ring interface during rotation. The nature of this interface means it must allow for the *c*-ring to rotate against subunit *a*, but not permit proton leakage, especially if operating close to equilibrium (free energy of ATP hydrolysis approximately the same as the energy of established pH gradient), where a back flow of protons could occur. Moreover, the generation of a pH gradient results in an increased backward rotation pressure on the V-ATPase and a fall in the ATP/ADP ratio equilibrium can result in the proton motive force exceeding the free energy of ATP hydrolysis. The ability of an inactive V-ATPase to still maintain a high proton gradient means that the *c*-ring/*a*-subunit interface must not allow for the back flow of protons when there is a fall in the ATP/ADP ratio. This resistance to backwards rotation occurs through an as yet undetermined process, however the presence of this linkage may act as a "ratchet mechanism," permitting rotation in pump mode but stopping rotation in synthesis mode, allowing for the build up of a proton gradient. The apparent flexibility inherent within the V-ATPase system[22] during catalysis can move the stator connection away from the *c*-ring/rotor axle and would permit proton translocation. Upon the lowering of the cellular ATP/ADP ratio, the stator would adopt the position seen in the apparent "low energy/low ATP" ground state (Fig. 1), which would stop proton leakage through reverse rotation of the *c*-ring.

The V-ATPase has been shown to be regulated through a process which involves the dissociation of V_1 from V_o.[38,39] Electron microscopy studies on the V-ATPase and tomographic studies on the A-ATPase which has been primed for dissociation through changes in pH and temperature have shown a large 30° angular tilt. The linkage present between stator 1 and the central rotor axle/*c*-ring may play a role in this process in tethering V_1 to V_o. Alternatively it may play a role in re-association of the V-ATPase complex, a process which is currently poorly understood. FFEA can provide insight into this process through simulation of the dissociation of the V_o and V_1 domains and the C subunit. Figure 15 shows an example trajectory of such a system. Interestingly, the model predicts the departure of subunit C from the complex before full dissociation occurs, which is consistent with subunit C being implicitly involved in this process as it is predicted to, in response to cellular signals, be removed from the complex causing dissociation. Moreover the stator elements show apparent rigidity in the dissociated complex as shown in the cryo-EM reconstruction of the isolated V_1 domain.[40,41] This demonstrates the capabilities of FFEA in the simulation of large biomolecular non-covalent complexes. Further biochemical studies will be required to test each of the discussed hypotheses and reveal the role of the apparent stator rotor axle/*c*-ring connection.

CONCLUSION

Here we have shown how both ENM and continuum FFEA simulations can be used to simulate the intrinsic flexibility within the ATPase family of rotary motors. Moreover, we have shown that the apparent connectivity between the stator network and the central rotor axle of c-ring acts to both restrict rotation and limit the available flexibility within the system. The additional flexing seen upon the breakage of this connection may be used to accommodate the cycling between the different ATP bound states of the A_1/V_1 motor, in particular that of the open state which adopts a lower position. Further biochemical studies are currently underway, guided by the information obtained from the simulations which will further characterize the linkage between the stator network and the axle and rotor ring and test that this is not an artifact of the electron microscopy experiment.

REFERENCES

1. Muench SP, Trinick J, Harrison MA. Structural divergence of the rotary ATPases. Q Rev Biophys 2011;44:311–356.

2. Imamura H, Nakano M, Noji H, Muneyuki E, Ohkuma S, Yoshida M, Yokoyama K. Evidence for rotation of V1-ATPase. Proc Natl Acad Sci USA 2003;100:2312–2315.

3. Noji H, Yasuda R, Yoshida M, Kinosita K, Jr. Direct observation of the rotation of F1-ATPase. Nature 1997;386:299–302.

4. Boyer PD. The ATP synthase—a splendid molecular machine. Annu Rev Biochem 1997;66:717–749.

5. Sambongi Y, Iko Y, Tanabe M, Omote H, Iwamoto-Kihara A, Ueda I, Yanagida T, Wada Y, Futai M. Mechanical rotation of the c subunit oligomer in ATP synthase (F0F1): direct observation. Science 1999;286:1722–1724.

6. Yokoyama K, Nakano M, Imamura H, Yoshida M, Tamakoshi M. Rotation of the proteolipid ring in the V-ATPase. J Biol Chem 2003;278:24255–24258.

7. Mitome N, Suzuki T, Hayashi S, Yoshida M. Thermophilic ATP synthase has a decamer c-ring: indication of noninteger 10:3 H+/ATP ratio and permissive elastic coupling. Proc Natl Acad Sci USA 2004; 101:12159–12164.

8. Pogoryelov D, Reichen C, Klyszejko AL, Brunisholz R, Muller DJ, Dimroth P, Meier T. The oligomeric state of c rings from cyanobacterial F-ATP synthases varies from 13 to 15. J Bacteriol 2007;189:5895–5902.

9. Vollmar M, Schlieper D, Winn M, Buchner C, Groth G. Structure of the c(14) rotor ring of the proton translocating chloroplast ATP synthase. J Biol Chem 2009;284:18228–18235.

10. Meier T, Polzer P, Diederichs K, Welte W, Dimroth P. Structure of the rotor ring of F-type Na+-ATPase from *Ilyobacter tartaricus*. Science 2005;308:659–662.

11. Pogoryelov D, Yu J, Meier T, Vonck J, Dimroth P, Muller DJ. The c15 ring of the *Spirulina platensis* F-ATP synthase: F1/F0 symmetry mismatch is not obligatory. EMBO Rep 2005;6:1040–1044.

12. Cherepanov DA, Mulkidjanian AY, Junge W. Transient accumulation of elastic energy in proton translocating ATP synthase. FEBS Lett 1999;449:1–6.

13. Grabe M, Wang H, Oster G. The mechanochemistry of V-ATPase proton pumps. Biophys J 2000;78:2798–813.

14. Junge W, Sielaff H, Engelbrecht S. Torque generation and elastic power transmission in the rotary F(O)F(1)-ATPase. Nature 2009;459:364–370.

15. Sielaff H, Rennekamp H, Wachter A, Xie H, Hilbers F, Feldbauer K, Dunn SD, Engelbrecht S, Junge W. Domain compliance and elastic power transmission in rotary F(O)F(1)-ATPase. Proc Natl Acad Sci USA 2008;105:17760–17765.

16. Wachter A, Bi Y, Dunn SD, Cain BD, Sielaff H, Wintermann F, Engelbrecht S, Junge W. Two rotary motors in F-ATP synthase are elastically coupled by a flexible rotor and a stiff stator stalk. Proc Natl Acad Sci USA 2011;108:3924–3929.

17. Balakrishna AM, Hunke C, Gruber G. The structure of subunit E of the *Pyrococcus horikoshii* OT3 A-ATP synthase gives insight into the elasticity of the peripheral stalk. J Mol Biol 2012;420:155–163.

18. Bernal RA, Stock D. Three-dimensional structure of the intact *Thermus thermophilus* H+-ATPase/synthase by electron microscopy. Structure 2004;12:1789–98.

19. Bottcher B, Bertsche I, Reuter R, Graber P. Direct visualisation of conformational changes in EF(0)F(1) by electron microscopy. J Mol Biol 2000;296:449–457.

20. Matthies D, Haberstock S, Joos F, Dotsch V, Vonck J, Bernhard F, Meier T. Cell-free expression and assembly of ATP synthase. J Mol Biol 2011;413:593–603.

21. Stewart AG, Lee LK, Donohoe M, Chaston JJ, Stock D. The dynamic stator stalk of rotary ATPases. Nat Commun 2012;3:687.

22. Song CF, Papachristos K, Rawson S, Huss M, Wieczorek H, Paci E, Trinick J, Harrison MA, Muench SP. Flexibility within the Rotor and Stators of the Vacuolar H+-ATPase. PLOS ONE 2013;8(12).

23. Tirion MM. Large amplitude elastic motions in proteins from a single-parameter, atomic analysis. Phys Rev Lett 1996;77:1905–1908.

24. Chacon P, Tama F, Wriggers W. Mega-Dalton biomolecular motion captured from electron microscopy reconstructions. J Mol Biol 2003;326:485–492.

25. Tama F, Wriggers W, Brooks CL, III. Exploring global distortions of biological macromolecules and assemblies from low-resolution structural information and elastic network theory. J Mol Biol 2002; 321:297–305.

26. Oliver RC, Read DJ, Harlen OG, Harris SA. A stochastic finite element model for the dynamics of globular macromolecules. J Comp Phys 2013;239:147–165.

27. Schöberl J. NETGEN - an advancing front 2d/3d-mesh generator based on abstract rules. Computing and visualization in science 1997;1:41–52.

28. Radmacher M, Fritz M, Cleveland JP, Walters DA, Hansma PK. Imaging adhesion forces and elasticity of lysozyme adsorbed on mica with the atomic force microscope. Langmuir 1994;10:3809–3814.

29. Fischer H, Polikarpov I, Craievich AF. Average protein density is a molecular weight dependent function. Protein Science 2004;13:2825–2828.

30. Quillin ML, Matthews BW. Accurate calculation of the density of proteins. Acta Crystallogr Sect D: Biol Crystallogr 2000;56:791–794.

31. Wriggers W, Milligan RA, Schulten K, McCammon JA. Self-organizing neural networks bridge the biomolecular resolution gap. J Mol Biol 1998;284:1247–1254.

32. Stember JN, Wriggers W. Bend-twist-stretch model for coarse elastic network simulation of biomolecular motion. J Chem Phys 2009;131:074112.

33. Meyer T, Ferrer-Costa C, Perez A, Rueda M, Bidon-Chanal A, Luque FJ, Laughton CA, Orozco M. Essential dynamics: A tool for efficient trajectory compression and management. J Chem Theory Comput 2006;2:251–258.

34. Lau WCY, Rubinstein JL. Structure of intact *Thermus thermophilus* V-ATPase by cryo-EM reveals organization of the membrane-bound VO motor. Proc Natl Acad Sci USA 2010;107:1367–1372.

35. Muench SP, Huss M, Song CF, Phillips C, Wieczorek H, Trinick J, Harrison MA. Cryo-electron microscopy of the vacuolar ATPase motor reveals its mechanical and regulatory complexity. J Mol Biol 2009;386:989–999.

36. Benlekbir S, Bueler SA, Rubinstein JL. Structure of the vacuolar-type ATPase from *Saccharomyces cerevisiae* at 11-angstrom resolution. Nat Struct Mol Biol 2012;19:1356.

37. Lau WCY, Rubinstein JL. Subnanometre-resolution structure of the intact *Thermus thermophilus* H+-driven ATP synthase. Nature 2012; 481(7380):214.

38. Kane PM. Disassembly and reassembly of the yeast vacuolar H(+)-ATPase in vivo. J Biol Chem 1995;270:17025–17032.

39. Sumner JP, Dow JA, Earley FG, Klein U, Jager D, Wieczorek H. Regulation of plasma membrane V-ATPase activity by dissociation of peripheral subunits. J Biol Chem 1995;270:5649–5653.

40. Muench SP, Scheres SH, Huss M, Phillips C, Vitavska O, Wieczorek H, Trinick J, Harrison MA. Subunit positioning and stator filament stiffness in regulation and power transmission in the V1 motor of the *Manduca sexta* V-ATPase. J Mol Biol 2014; 426:286–300.

41. Tabke K, Albertmelcher A, Vitavska O, Huss M, Schmitz HP, Wieczorek H. Reversible disassembly of the yeast V-ATPase revisited under in vivo conditions. Biochem J 2014;462:185–197.